EUROPEAN ORGANIZATION FOR NUCLEAR RESEARCH

$f_0(980)$ production in inelastic pp collisions at $\sqrt{s} = 5.02$ TeV

ALICE Collaboration

Abstract

The measurement of the production of $f_0(980)$ in inelastic pp collisions at $\sqrt{s} = 5.02$ TeV is presented. This is the first reported measurement of inclusive $f_0(980)$ yield at LHC energies. The production is measured at midrapidity, $|y| < 0.5$, in a wide transverse momentum range, $0 < p_T < 16$ GeV/c, by reconstructing the resonance in the $f_0(980) \to \pi^+\pi^-$ hadronic decay channel using the ALICE detector. The p_T-differential yields are compared to those of pions, protons and ϕ mesons as well as to predictions from the HERWIG 7.2 QCD-inspired Monte Carlo event generator and calculations from a coalescence model that uses the AMPT model as an input. The ratio of the p_T-integrated yield of $f_0(980)$ relative to pions is compared to measurements in e^+e^- and pp collisions at lower energies and predictions from statistical hadronisation models and HERWIG 7.2. A mild collision energy dependence of the $f_0(980)$ to pion production is observed in pp collisions from SPS to LHC energies. All considered models underpredict the p_T-integrated $f_0(980)/(\pi^+ + \pi^-)$ ratio. The prediction from the canonical statistical hadronisation model assuming a zero total strangeness content of $f_0(980)$ is consistent with the data within 1.9σ and is the closest to the data. The results provide an essential reference for future measurements of the particle yield and nuclear modification in p–Pb and Pb–Pb collisions, which have been proposed to be instrumental to probe the elusive nature and quark composition of the $f_0(980)$ scalar meson.

1 Introduction

The conventional picture for the classification of hadrons is based on the constituent quark model introduced in the 1960s [1], in which the observed mesons and baryons are described as colourless q$\bar{\text{q}}$ and qqq bound states, respectively. Most of the known observed states fit into the quark model picture. At the same time, there are states whose quantum numbers are known but their mass and width have not been measured, and observed resonances whose properties suggest an exotic structure [2]. One remarkable case is that of the light scalar mesons, light-flavoured states with spin zero, positive parity and charge ($J^{PC} = 0^{++}$) and masses below 2 GeV/c^2, whose identification represents a long-standing puzzle in particle physics [3–8]. From a theoretical point of view, the structure of these states is highly debated [9]: light scalar mesons could be conventional q$\bar{\text{q}}$ mesons, or compact (qq)($\overline{\text{qq}}$) structures (tetraquarks), or meson–meson bound states in the form of hadronic molecules, or a superposition of all these components.

From an experimental point of view, light scalar resonances are typically reconstructed via their dominant decay channels into pseudoscalar mesons (e.g., $\pi\pi$, $\eta\pi$, $\eta\eta$...). The states decaying into pions, in particular, have large characteristic decay widths, of the order of few tens to few hundreds of MeV/c^2, due to the large available phase space. Therefore, the isolation of the particle signals is particularly challenging as broad signals strongly overlap. In addition, for some of the scalar meson states, different decay channels can open up within a short mass interval and distort the line shapes of the nearby resonances.

Among the scalar mesons, the f$_0$(980) state is particularly interesting for two reasons. First, despite a long history of experimental and theoretical studies, its nature is still controversial as the properties of the f$_0$(980) state are compatible with a conventional q$\bar{\text{q}}$ meson [10], a tetraquark [11], and a K$\overline{\text{K}}$ molecular [12] structure. Secondly, the f$_0$(980) represents an interesting probe of the high-density hadronic final state of heavy-ion collisions and in-medium particle formation mechanisms [13].

The f$_0$(980) couples predominantly to the $\pi\pi$ and K$\overline{\text{K}}$ channels and the background is mainly given by the f$_0$(500) and the f$_0$(1270), among the scalar mesons. An indication in favour of the tetraquark structure of f$_0$(980) [14] comes from measurements of the ϕ meson radiative decays by SND [15], CMD2 [16], and KLOE [17, 18] experiments. This is further supported by a recent analysis [11] of the J/ψ radiative decay data from BESIII [11, 19]. The f$_0$(980) is also prominently produced in D$_s^+$ decays as reported by the E791 collaboration [20], and observed in weak decays of B and B$_s$ mesons measured with LHCb [21, 22]. There, the appearance of the f$_0$(980) in competition with the ϕ meson in these decays could be explained by a large s$\bar{\text{s}}$ component of this state, combined with the fact that the c $\rightarrow$ s coupling is Cabibbo favoured. In this scenario, the structure of the f$_0$(980) would be $|\text{f}_0(980)\rangle = |(\text{u}\bar{\text{u}} + \text{d}\bar{\text{d}})\text{s}\bar{\text{s}}\rangle/\sqrt{2}$ [2]. An analysis of the measured couplings of the B and B$_s$ mesons to J/ψ+f$_0$(980) excluded the tetraquark hypothesis [22], a conclusion that is however challenged by a different analysis of the same data [23]. Indications that f$_0$(980) could be a K$\overline{\text{K}}$ come instead from the study of pion–pion and kaon–kaon scattering via nonperturbative QCD methods, which use effective meson-exchange models of the $\pi\pi$ interaction [24, 25] and study the K$\overline{\text{K}}$ interaction for coupled and single channels in chiral effective theory [12, 26].

In addition to measuring the production rates and branching fractions of f$_0$(980) in ϕ and heavy-flavour decays, several authors [7, 27–29] have proposed to investigate its nature by using heavy-ion collisions and exploiting the unique production (and decay) environment accessible in these reactions. In high-energy heavy-ion collisions, two extreme states of matter are reached one after the other. If enough energy is deposited in the collision region, the state of deconfined strongly interacting matter called quark–gluon plasma (QGP) is produced and expands as a nearly perfect liquid until the temperature reaches the pseudo-critical value of $\approx$ 155 MeV [30] and a transition to confined QCD matter takes place. A hot (T $\approx$ 100–150 MeV) and dense gas of interacting hadrons is formed in which resonances decay and particles interact (pseudo)elastically until they decouple. At the LHC, the system produced in Pb–Pb collisions decouples after about 10 fm/c [31] and the production of hadronic resonances with

lifetimes of the order of 1 to 10 fm/c is studied to characterise the hadronic stage of the collision [32–34]. With its width between 10 and 100 MeV/c^2 and a corresponding lifetime of $\approx$ 5–10 fm/c, the $f_0(980)$ is a probe for the dense hadron gas formed in the late stage of heavy-ion collisions [13].

Measurements of the nuclear modification factor [27], the particle yield per event [28], and the elliptic flow coefficient [29] have been suggested to provide insights into the internal structure of the $f_0(980)$. Models of hadron formation via recombination (coalescence) [35–37] of quarks in the quark–gluon plasma that have been successful in describing LHC data, indicate that the $f_0(980)$ production in the intermediate transverse momentum range ($2 < p_T < 5$ GeV/c) is sensitive to the number of constituent quarks. Theory calculations based on a coalescence model [28] show that the p_T-integrated production of $f_0(980)$ in central heavy-ion collisions at LHC energies is expected to be two orders of magnitude lower if the state has a tetraquark structure compared to the results for a non-exotic diquark structure q$\bar{q}$, or a hadronic molecule configuration. On the other hand, the production of a tetraquark state would be enhanced in heavy-ion collisions with respect to pp collisions at the same energy in the $\approx$ 2–6 GeV/c momentum range [7, 27]. Measurements of the nuclear modification factor [7, 27] or of the p_T-dependent yield ratio of the $f_0(980)$ to particles with different (but established) quark content could therefore shed light on the nature of the state. The authors of [29] also suggest that the azimuthal production asymmetry in the $f_0(980)$ momentum distributions, quantified by the elliptic flow coefficient, could be sensitive to the number of constituent quarks in the kinematic range in which hadron formation occurs predominantly via quark recombination (coalescence). A measurement of the $f_0(980)$ production in pp collisions is necessary for the determination of the nuclear modification factor and constitutes a reference for the study of the particle production in heavy-ion collisions.

In this letter, the first measurement of the inclusive production of $f_0(980)$ in inelastic pp collisions at the LHC is reported. To provide a baseline for studies in heavy-ion interactions, the data using collisions at $\sqrt{s} = 5.02$ TeV were analysed, corresponding to the centre-of-mass energy per nucleon of the p–Pb and Pb–Pb data samples collected during the LHC Run 2. Measurements of $f_0(980)$ in p–Pb and Pb–Pb collisions at this energy will be the subject of future publications. The production of $f_0(980)$ is measured at midrapidity, $|y| < 0.5$, in a broad transverse momentum range between 0 and 16 GeV/c. An overview of the ALICE experimental setup is given in Sec. 2, followed by a description of the analysis strategy in Sec. 3. This includes details on the data sample, the $f_0(980)$ signal reconstruction, the yield extraction and corrections, and the systematic uncertainty estimation. Results are discussed in comparison to lower energy data and theoretical models in Sec. 4, while in Sec. 5 the conclusions are summarised.

2   Experimental setup

The experimental setup and details on the performance of the ALICE detector are described in Refs. [38, 39]. The ALICE detector consists of a central barrel with a set of detectors devoted to the reconstruction and identification of the charged particles, a forward muon spectrometer and a set of backward and forward systems for triggering and event characterisation purposes. The central barrel detectors are located inside a solenoidal magnet that provides a magnetic field of 0.5 T. The main detectors employed for the analysis presented in this work are the V0, the Inner Tracking System (ITS), the Time Projection Chamber (TPC), and the Time-of-Flight detector (TOF). The V0 consists of two scintillator arrays placed on both sides of the interaction point covering the pseudorapidity regions $2.8 < \eta < 5.1$ (V0A) and $-3.4 < \eta < -1.7$ (V0C), respectively. The V0 provides the minimum bias trigger of the experiment and is used for suppressing beam-induced background at the offline analysis level. The position of the collision vertex and the tracks of charged particles are reconstructed in the central barrel using the ITS and the TPC. The ITS is a high-resolution tracker that consists of six cylindrical layers of silicon detectors. The TPC is a large cylindrical drift detector covering a radial distance of $85 < r < 247$ cm from the beam axis and having longitudinal dimensions of about -250 $< z <$ 250 cm. The TOF is a large area array of multigap resistive plate chambers, placed at a radius of about 370–399 cm from the beam

line. In the central barrel, charged particles can be identified via measurements of their specific energy loss, dE/dx, provided by the TPC with a resolution of 5%, and via their time-of-flight measured by the TOF with a resolution of about 80 ps.

3   Data analysis

The measurement of f$_0$(980) production is performed using a sample of minimum bias pp collision events at a centre-of-mass energy of $\sqrt{s}$ = 5.02 TeV, collected in the years 2015 and 2017. The minimum-bias trigger requires at least one hit in both V0A and V0C detectors [40]. The integrated luminosity after trigger selection is $\approx$ 21.8 nb^{-1}. Events are selected for the analysis if the position of the reconstructed collision vertex along the beam axis is located within 10 cm from the nominal interaction point. To reduce the pileup caused by multiple interactions in the same bunch crossing, a criterion based on the offline reconstruction of multiple primary vertices in the two innermost layers of the ITS, namely the Silicon Pixel Detector (SPD) is applied [38]. The rejected events account for less than 1% of the total events. After applying these selection criteria, $\approx 9.14 \times 10^8$ collision events have been analysed.

The f$_0$(980) resonance signal is reconstructed via its decay into a pair of oppositely charged pions, f$_0$(980) $\rightarrow \pi^+\pi^-$. This requires the reconstruction, selection and identification of pion tracks in the central barrel of ALICE. To ensure a uniform detector acceptance, only charged tracks with $p_T > 0.15$ GeV/c and pseudorapidity $|\eta| < 0.8$ are considered for the analysis. Track selection criteria are applied to the charged tracks as in previous works [32, 33] to ensure a good quality of the reconstruction. To this end, each track in the TPC is required to have crossed at least 70 readout pad rows out of a maximum possible 159. To reduce the contamination from secondary particles, tracks are accepted if their distance of closest approach to the collision vertex in the longitudinal (d_z) and transverse (d_{xy}) directions satisfy $d_z < 2$ and $d_{xy} < 0.0105 + 0.0350 \times p_T^{-1.1}$, where p_T and distance are in units of GeV/c and cm, respectively.

The identification of pions is performed using the TPC and the TOF detectors and criteria based on the difference between the measured and expected signals for a given particle hypothesis, divided by the resolution (σ_{TPC}, σ_{TOF}). In the TPC, charged particles are identified as π if the measured dE/dx is compatible with the expected pion mean specific energy loss within two standard deviations ($2\sigma_{TPC}$) over the entire momentum range. If a measurement of the particle time-of-flight by the TOF is available, a TOF-based $3\sigma_{TOF}$ selection criterion is applied on top of the TPC-based one, over the measured momentum range.

3.1   Raw yield extraction

The f$_0$(980) resonance signal is reconstructed via an invariant mass analysis by combining oppositely-charged pions within the same event into pairs and imposing the pair to have a rapidity within the range $|y| < 0.5$. To remove the combinatorial background, the like-sign method is employed. The same-charge pion tracks from the same event are combined into $\pi^+\pi^+$ and $\pi^-\pi^-$ pairs. The total like-sign invariant mass distribution is calculated as the geometric mean of the positively-charged and negatively-charged pair distributions, as $2\sqrt{N^{++}N^{--}}$, where N^{++} and N^{--} are the number of $\pi^+\pi^+$ and $\pi^-\pi^-$ pairs, respectively. The $\pi^+\pi^-$ and like-sign background invariant mass distributions are extracted for various intervals of the pair p_T, and for each of these, the like-sign background is subtracted from the unlike-sign pair distribution. After the subtraction of the combinatorial background, the f$_0$(980) signal peak, sitting on the right-hand tail of the broad ρ(770) meson signal, is visible on top of a residual background. Two examples of the $\pi^+\pi^-$ invariant mass distributions after combinatorial background subtraction are shown in Fig. 1 for a low-p_T and for a high-p_T interval. With increasing p_T, the significance of the f$_2$(1270) resonance signal increases and the broad f$_2$(1270) peak becomes visible on the right side of the f$_0$(980) signal. The residual background originates from correlated $\pi^+\pi^-$ pairs from mini-jets and from misidentified particles. The main contributions to the correlated background arise from the decay of the
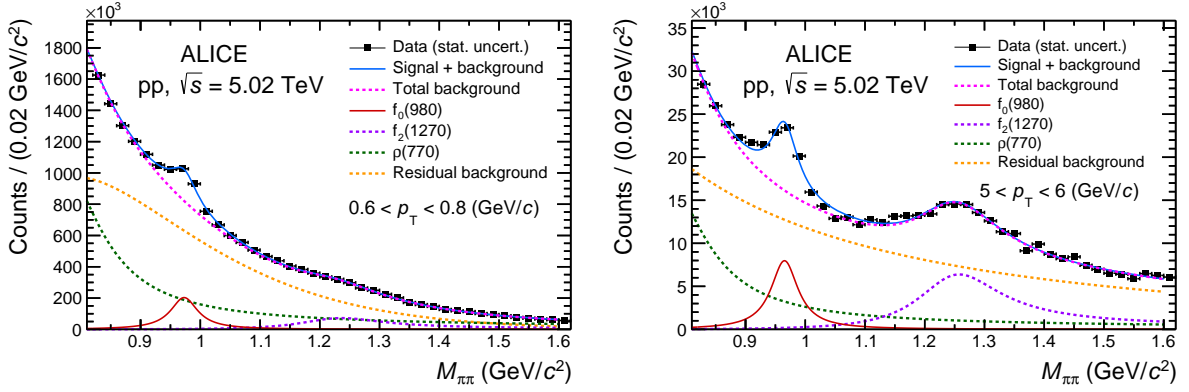
Figure 1: Left (right) plot shows the invariant mass distribution of $\pi^+\pi^-$ pairs after like-sign background subtraction in low (high) transverse-momentum interval in pp collisions at $\sqrt{s} = 5.02$ TeV in $|y| < 0.5$. Solid blue curves represent fits with the function shown in Eq. 1 and a residual background shown in Eq. 3. Solid red curve represent $f_0(980)$ signal while other dashed curves represent the background contributions from $\rho(770)$, $f_2(1270)$ and residual background.

$\rho(770)$ and the $f_2(1270)$ resonances into oppositely-charged π pairs. In order to extract the $f_0(980)$ yields in each p_T interval, the distributions are fitted in the invariant mass interval $0.8 < M_{\pi\pi} < 1.6$ GeV/c^2 with a function that is the sum of three relativistic Breit-Wigner functions (rBW) describing the $\rho(770)$, $f_0(980)$ and $f_2(1270)$ signals [32, 41, 42], and a residual background. Since the resolution on the invariant mass is negligible with respect to the natural width of the considered resonances, the resonance shape can be modelled with a rBR with no need for any additional Gaussian smearing to account for detector resolution effects. Each of the rBW functions is defined as

$$\text{rBW}(M_{\pi\pi}) = \frac{AM_{\pi\pi}\Gamma(M_{\pi\pi})M_0}{(M_{\pi\pi}^2 - M_0^2)^2 + M_0^2\Gamma^2(M_{\pi\pi})} \tag{1}$$

where $\Gamma(M_{\pi\pi})$ is given by

$$\Gamma(M_{\pi\pi}) = \left[\frac{(M_{\pi\pi}^2 - 4m_\pi^2)}{(M_0^2 - 4m_\pi^2)}\right]^{(2J+1)/2} \times \frac{\Gamma_0 M_0}{M_{\pi\pi}}. \tag{2}$$

Here, A is the normalisation constant, M_0 and Γ_0 are the rest mass and width of the resonance, m_π is the charged pion mass and the spin is $J = 0$ for $f_0(980)$, $J = 1$ for $\rho(770)$ and $J = 2$ for $f_2(1270)$. The shape of the residual background resembles that of a Maxwell-Boltzmann distribution and therefore it is fitted with a similar functional form $f_{\text{bg}}(M_{\pi\pi})$ [34]

$$f_{\text{bg}}(M_{\pi\pi}) = \sqrt{(m_{\pi\pi} - m_{\text{cutoff}})^n} \, C^{3/2} \, \exp\left[-C(m_{\pi\pi} - m_{\text{cutoff}})^n\right], \tag{3}$$

where m_{cutoff} is the low-mass cutoff expected to be equal to the rest mass of the $\pi^+\pi^-$ pair.

For the extraction of the particle yields, the fits are performed with the following configuration of the fit parameters. The mass and the width of the $\rho(770)$, and the width of the $f_2(1270)$ are fixed to their vacuum values, $m_\rho = 775.26$ MeV/c^2, $\Gamma_\rho = 149.1$ MeV/c^2, and $\Gamma_{f_2} = 186.7$ MeV/c^2 [2]. The width of the $f_0(980)$ is fixed to the average value of the range reported in Ref. [2] that corresponds to $\Gamma_{f_0} = 0.055$ GeV/c^2. The masses of the $f_0(980)$ and the $f_2(1270)$, as well as the m_{cutoff}, C and n parameters of f_{bg} are left free. The fit parameter configuration has been varied to take into account possible imperfections in the description of the background and signal shapes, as discussed in Section 3.3. In Fig. 1, the fit result to

the invariant mass distribution of $\pi^+\pi^-$ pairs after like-sign background subtraction is shown for two p_T intervals, namely $0.6 < p_T < 0.8$ GeV/c and $5 < p_T < 6$ GeV/c.

3.2 Yield corrections

In order to obtain the f$_0$(980) production yield per unit of rapidity and p_T per inelastic event $\left(\frac{1}{N_{INEL}}\frac{d^2N}{dyd p_T}\right)$, several correction factors are applied to the raw yields obtained from the fit procedure in each p_T interval according to the following formula

$$\frac{1}{N_{INEL}}\frac{d^2N}{dp_T dy} = \frac{1}{N_{evt}}\frac{N_{f_0(980)\to\pi\pi}}{\Delta p_T \Delta y}\frac{\varepsilon_{trig}\,\varepsilon_{vtx}}{A\times\varepsilon_{rec}}\frac{f_{sig}}{BR}. \tag{4}$$

Here, $N_{f_0(980)\to\pi\pi}$ is the f$_0$(980) raw yield measured in a given rapidity (Δy) and transverse momentum (Δp_T) interval, N_{evt} is the number of collision events that satisfy the selection criteria. The minimum-bias trigger efficiency, the vertex reconstruction efficiency and the signal loss correction factor are represented by ε_{trig}, ε_{vtx} and f_{sig}, respectively. The branching ratio correction amounts to BR = $(46 \pm 6)\%$ [43] assuming dominance of $\pi\pi$ and KK channels. The yields of f$_0$(980) are normalised to the number of inelastic pp collisions with a trigger efficiency correction, $\varepsilon_{trig} = 0.757 \pm 0.019$ [44, 45], which takes into account the efficiency of the V0-based trigger to select inelastic events. The vertex reconstruction efficiency in pp collisions at $\sqrt{s} = 5.02$ TeV is found to be $\varepsilon_{vtx} = 0.958$ [33]. The $A \times \varepsilon_{rec}$ factor corrects for the detector acceptance times the f$_0$(980) reconstruction efficiency and is evaluated using a detailed Monte Carlo simulation of the ALICE detector geometry, material, and response. The pp collision events are simulated using the PYTHIA 8 event generator [46] with the addition of the f$_0$(980) signals. The generated particles in the simulation are propagated through the detector using GEANT3 [47]. The $A \times \varepsilon_{rec}$ is calculated in the rapidity range $|y| < 0.5$ as a function of p_T and is defined as the ratio of the number of reconstructed and generated f$_0$(980). The reconstruction of f$_0$(980) in the simulation is performed using the same event and track selection criteria as employed for the analysis of the data.

The signal loss correction factor, f_{sig}, accounts for the fraction of f$_0$(980) signal lost due to trigger inefficiencies and can be determined as a function of p_T using Monte Carlo simulations. Because a simulation with injected f$_0$(980) signals may not lead to a realistic estimate of this correction factor, the correction is taken to be the same as for the ϕ meson at the same collision energy. The earlier analysis in [33] showed that this correction does not depend significantly on the particle mass for resonances decaying strongly into two charged particles. This factor ranges between 1.07 for $0 < p_T < 0.2$ GeV/c and 1 for $p_T > 2.5$ GeV/c.

3.3 Systematic uncertainties

The sources of systematic uncertainty in the measurement of the f$_0$(980) yields are summarised in Table 1. These include yield extraction, track and event selection, global tracking efficiency, particle identification, the knowledge of the ALICE material budget, and that of the hadron interaction cross section in the detector material. The estimated values of the uncertainties are reported in Table 1 for low, intermediate and high-p_T intervals. The systematic uncertainty associated with the yield extraction arises from the fit procedure and is determined by varying the fitting range as well as the signal and the residual background fit parameters. In particular, the width of the f$_0$(980) was varied by sampling the range from 10 to 100 MeV/c^2 given in [2] and the width of the f$_2$(1270) was varied within ± 7.5 MeV/c^2 that corresponds to a $\pm 3\sigma$ range of the width value reported in [2]. These variations result in the largest contribution to the uncertainty on the yield extraction. The uncertainties due to the yield extraction are p_T dependent and vary from 7.1% in the lowest p_T interval, to 15.3% in the highest p_T interval of this analysis. The systematic uncertainty due to the track selection is evaluated by varying a single track selection criterion at a time in both data and simulation, and by repeating all the steps of the analysis. This contribution ranges from 9.3% to 2.1% from low to high p_T. The difference in the efficiency of the matching of TPC tracks to ITS clusters (global tracking efficiency) between data and simulations results

Table 1: Contributions to the relative systematic uncertainty of the p_T-dependent yield of $f_0(980)$ in pp collisions at $\sqrt{s} = 5.02$ TeV. The uncertainties are given for the lowest and the highest p_T intervals of the measured spectrum as well as for one intermediate p_T interval. The total uncertainty is obtained as the sum in the quadrature of the individual contributions. Values are expressed in percentage (%).

Source of uncertainty	p_T (GeV/c)		
	0–0.2	4–4.5	12–16
Yield extraction	7.1%	8.8%	15.3%
Track selection	9.3%	2.2%	2.1%
Global tracking efficiency	2%	4%	4%
Particle identification	6.8%	1.5%	6%
Event selection	7.6%	2.1%	3.3%
Material budget	5.2%	0%	0%
Hadronic interaction	3.4%	0%	0%
Total	16.8%	10.2%	17.4%

in a contribution to the systematic uncertainty of 2–4% depending on p_T. The systematic uncertainty associated with the particle identification is due to an imperfection in the description of the dE/dx in the TPC-based $n\sigma$ selection in the Monte Carlo simulation as compared to data. The $n\sigma$ selection is varied in data and simulation simultaneously to a $3\sigma_{TPC}$ particle identification criterion and results in a p_T-dependent relative systematic uncertainty of 1.5–6.8%. The choice of the event selection criteria leads to a systematic uncertainty of 2.1–7.6%. The systematic uncertainty associated with the signal loss correction is estimated by comparing the correction for ϕ mesons, used as a proxy for $f_0(980)$, with that of other light-flavour hadrons and is found to be lower than 1%. Finally, the uncertainty on the knowledge of the ALICE material budget and that of the hadron interaction cross section in the detector material leads to a systematic uncertainty lower than 5.3% and 3.4%, respectively [39, 48, 49]. The total relative systematic uncertainty is obtained as the sum in the quadrature of these contributions.

4   Results and Discussion

The p_T-differential yield of $f_0(980)$ for $|y| < 0.5$ in inelastic pp collisions at $\sqrt{s} = 5.02$ TeV is shown in the upper panel of Fig. 2. The measurement spans a wide p_T range from 0 to 16 GeV/c.

The normalisation and branching ratio relative uncertainties on the yields are independent of p_T and amount to 2.5% and 13%, respectively [43, 45].

At present, most of the Monte Carlo generators commonly employed to simulate pp collisions do not implement the generation of $f_0(980)$ in their default configurations. One notable exception is the HER-WIG 7.2 event generator [50, 51]. HERWIG 7.2 is a QCD-inspired Monte Carlo event generator that includes processes like initial and final state QCD radiation, a description of the underlying event via an eikonal multiple parton–parton interaction model, and a cluster hadronisation model for the formation of hadrons from the quarks and gluons produced in the parton shower. To allow for the comparison, model calculations have been performed in the same p_T intervals of the data. HERWIG fails to reproduce the data quantitatively, underestimating the measured yields by a factor of about (larger than) two at low and intermediate (high) p_T as it can be seen in the HERWIG/Data ratio shown in the middle panel of Fig. 2. The model reproduces at least qualitatively the shape of the p_T spectrum in the range $1 \leq p_T \leq 4$ GeV/c. At $p_T \geq 4$ GeV/c, HERWIG is not able to reproduce the data neither qualitatively nor quantitatively.

The data are also compared to a recent coalescence calculation [29, 52] that uses the AMPT multiphase transport model [52], coupled with a coalescence afterburner with Gaussian Wigner function to generate $f_0(980)$ in three configurations, i.e., as a $s\bar{s}$ meson, as a $u\bar{u}s\bar{s}$ tetraquark state, and as a K^+K^- molecule. The AMPT model contains four main components namely initial conditions, partonic interactions, con-
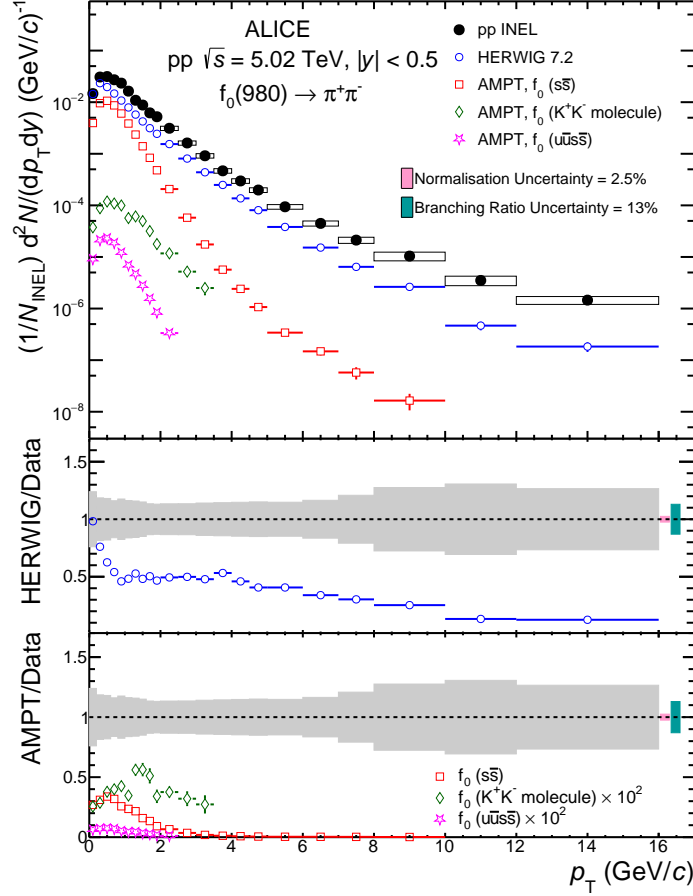
Figure 2: The p_T-differential yield of $f_0(980)$ in pp collisions at $\sqrt{s} = 5.02$ TeV is compared with predictions from the HERWIG 7.2 event generator [50, 51] and with a coalescence calculation [29] based on the AMPT model [52]. The statistical and systematic uncertainties on data (full black markers) are shown as bars and boxes, respectively. The middle and bottom panels show the model to data ratios. The grey boxes at unity represent the sum in quadrature of the statistical and systematic uncertainty on the data. The ratios of $u\bar{u}s\bar{s}$ tetraquark and K^+K^- molecule configurations from AMPT model predictions to data are multiplied by 100 to improve visibility. In all three panels, the uncertainties associated with the models are statistical ones.

version from partonic to hadronic matter, and interactions among hadrons based on a relativistic transport (ART) model [53, 54]. The initial conditions are obtained from the HIJING model [55] and the partonic interactions are determined according to the Zhang's Parton Cascade model [56]. In [29], the authors use the phase-space information of quarks from this stage to implement quark coalescence for the $f_0(980)$ with the $s\bar{s}$ and tetraquark configurations. In the default version of AMPT, the conversion of partons to hadrons is then calculated with the Lund string fragmentation [57–59], while in the string melting version of the model [60], a quark coalescence approach is used to combine partons to form hadrons. The phase-space information of kaons generated at this stage by AMPT is used as input for the coalescence afterburner for the $f_0(980)$ molecular state. As shown in Fig. 2, the $s\bar{s}$, the molecule, and the tetraquark configuration predictions underestimate the $f_0(980)$ p_T distribution by a factor of about three, and by two and three orders of magnitude, respectively. Note that the molecule and the tetraquark configuration prediction ratios to data are reported in the lowest panel of Fig. 2 multiplied by a factor of 100 to improve the visibility. In addition, the shape of the p_T spectra for the $s\bar{s}$ and the $u\bar{u}s\bar{s}$ tetraquark configurations are found to be significantly steeper than the measured one. Instead, the ratio between the model prediction
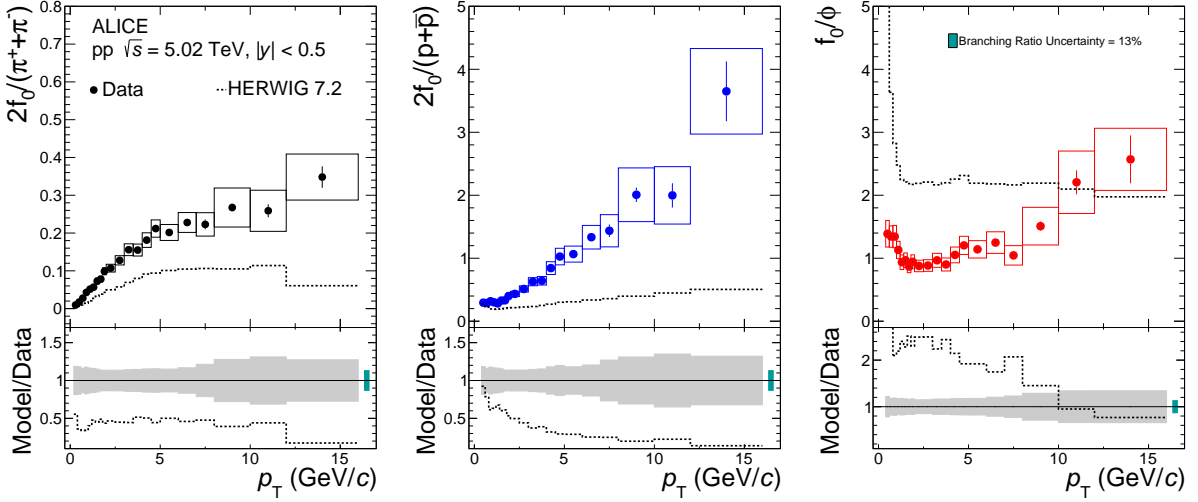
Figure 3: (Upper panels) Particle yield ratios of $f_0(980)$ to $\pi^+ + \pi^-$ [61] (left panel), $p + \bar{p}$ [61] (middle panel), and ϕ [33] (right panel) measured in inelastic pp collisions at $\sqrt{s} = 5.02$ TeV as a function of p_T. Data are compared to HERWIG 7.2 model predictions. The statistical and systematic uncertainties are shown as bars and boxes, respectively. (Lower panels) Ratio of measured particle ratios to the HERWIG model calculations (dashed line). The grey boxes at unity represent the sum in quadrature of the statistical and systematic uncertainty on the data. In the right panel, the ratio in the region for $p_T < 0.8$ GeV/c is off-scale. The relative uncertainty of 13% due to the branching ratio correction [43] is shown as a green box with an arbitrary horizontal width for visibility.

for the K^+K^- molecule configuration and the data exhibits a milder p_T dependence within uncertainties in the considered p_T range (0–3.5 GeV/c), indicating that in this configuration the model can reproduce qualitatively better the measured spectral shape.

The per-event p_T-integrated yield, dN/dy, and average transverse momentum, $\langle p_T \rangle$, are calculated by integrating the p_T-differential yield in the measured transverse momentum range. The obtained values are the following:

$$\frac{\mathrm{d}N}{\mathrm{d}y} = 0.0385 \pm 0.0001\,(\text{stat.}) \pm 0.0047\,(\text{syst.}) \tag{5}$$

$$\langle p_T \rangle = 0.9624 \pm 0.0014\,(\text{stat.}) \pm 0.0357\,(\text{syst.})\,\text{GeV/c} \tag{6}$$

Notably, the yield for $p_T > 16$ GeV/c has a negligible contribution to the dN/dy and thus no extrapolation was employed.

The production of $f_0(980)$ is compared to that of other light-flavour hadrons in Fig. 3 where the ratios of the $f_0(980)$ yields to those of $\pi^+ + \pi^-$ [61], $p+\bar{p}$ [61], and ϕ [33] measured in pp collisions at $\sqrt{s} = 5.02$ TeV are reported as a function of p_T. The ratio to $\pi^+ + \pi^-$ mesons exhibits an increasing trend as a function of p_T at low p_T and for $p_T > 5$ GeV/c it saturates within uncertainties.

The comparison of the production of $f_0(980)$ to that of protons and of the ϕ meson is particularly interesting as these particles have similar masses [2] but different quark content. In particular, the ϕ meson is a pure $s\bar{s}$ state, while the $f_0(980)$ contains a light flavour component ($u\bar{u}$, $d\bar{d}$) as well as a large $s\bar{s}$ component, as suggested by measurements of $f_0(980)$ produced in D_s^+ decays [20]. The $f_0(980)$ to $p + \bar{p}$ ratio shows an increasing monotonic trend as a function of p_T, whereas the $f_0(980)$ to ϕ ratio decreases for $p_T < 1.5$ GeV/c, remains flat till $p_T \simeq 8$ GeV/c, and increases for $p_T > 8$ GeV/c.

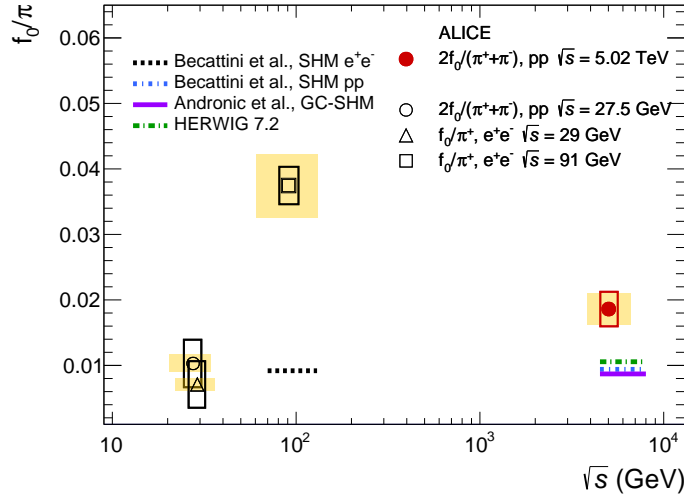The measured p_T-differential particle yield ratios are compared in Fig. 3 to the predictions from the

Figure 4: Comparison of the measured $2f_0/(\pi^+ + \pi^-)$ ratio with measurements in e^+e^- collisions at $\sqrt{s} = 29$ GeV [62], $\sqrt{s} = 91$ GeV [63] and in pp collisions at $\sqrt{s} = 27.5$ GeV [64]. The ratios are compared to predictions from statistical hadronisation model (SHM) calculations for e^+e^- collisions [65] and pp collisions [66], GC-SHM [67] and HERWIG 7.2 [50, 51]. The hollow boxes represent the total uncertainty on data. The relative uncertainty of 13% due to the branching ratio correction [43] applies to all data points and is shown as a yellow box. All error boxes are drawn with an arbitrary horizontal width for visibility.

HERWIG 7.2 event generator. The shape of the measured $2f_0(980)/(\pi^+ + \pi^-)$ ratio is fairly well reproduced over almost the entire measured p_T range, although the yield is underestimated by about a factor of two by the model. The model underestimates the $2f_0(980)/(p+\bar{p})$ ratio and fails to reproduce its p_T-dependence, with the measured ratio being more steeply increasing with p_T than the predicted one. The trend of $f_0(980)/\phi$ ratio is flat for $1 < p_T < 10$ GeV/c suggesting that its p_T dependence is qualitatively well reproduced by HERWIG in this momentum interval. However, the model overestimates the ratio by nearly a factor of two. For $p_T < 1$ GeV/c, the $f_0(980)/\phi$ ratio exhibits a steeply decreasing trend, that is qualitatively present also in the model prediction. At high p_T, the HERWIG predictions is consistent with the $f_0(980)/\phi$ data within the uncertainties.

The ratio of the p_T-integrated $f_0(980)$ yield relative to pions in pp collisions at $\sqrt{s} = 5.02$ TeV amounts to $2f_0/(\pi^+ + \pi^-) = (0.0186 \pm 0.0026)$, with the uncertainty being the sum in quadrature of the statistical and systematic uncertainties. The value is shown in Fig. 4 (red point) in comparison with results from measurements in pp and e^+e^- collisions at lower centre-of-mass energies as well as with model calculations.

The low energy experiment results were originally reported using different branching ratios, therefore all of them have been updated to take into account the most recent value of 46% [43] used in this letter. In Fig. 4, the same uncertainty on the BR is applied to all data points and reported as a shaded yellow box. The particle ratio value from the fixed-target NA27 experiment at the CERN SPS, measured in pp collisions at $\sqrt{s} = 27.5$ GeV [64] is 44.5% lower than the ratio measured at $\sqrt{s} = 5.02$ TeV, suggesting a mild increase of the $f_0(980)$ yield relative to pions with increasing energy of the pp collisions. The particle ratio values from e^+e^- collisions at $\sqrt{s} = 29$ GeV [62] and $\sqrt{s} = 91$ GeV [63] are lower by 61% and higher by a factor of two, respectively. The particle ratios are compared with predictions based on statistical hadronisation models [65–67] and the HERWIG 7.2 event generator. The statistical hadronisation model predictions by Becattini et al. for the e^+e^- case [65] and for the pp collisions [66] case underestimate the measurement by about a factor of two, similarly to a Grand Canonical formulation of the statistical hadronisation model (GC-SHM) from the GSI-Heidelberg group [67]. The value from
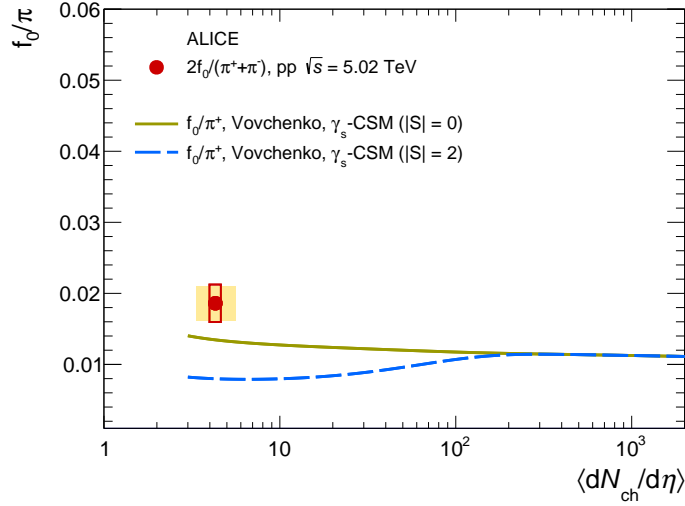
Figure 5: The $2f_0/(\pi^+ + \pi^-)$ ratio measured in pp collisions at $\sqrt{s} = 5.02$ TeV [61] is compared to two distinct predictions for f_0/π^+ from a canonical statistical model (γ_s-CSM [68], see text for details) as a function of $\langle dN_{\mathrm{ch}}/d\eta \rangle$. The two calculations differ by the assumed strangeness content of $f_0(980)$ and correspond to zero total strangeness, $|S| = 0$ and $|S| = 2$. The height of the hollow red box represents the total uncertainty on the ratio, its width represents the uncertainty on the $\langle dN_{\mathrm{ch}}/d\eta \rangle$. The relative uncertainty of 13% due to the branching ratio correction [43] is shown as a yellow box with an arbitrary horizontal width for visibility.

HERWIG is also a factor of about two lower than the measured ratio.

In Fig. 5, the measured p_{T}-integrated $2f_0/(\pi^+ + \pi^-)$ ratio in pp collisions at $\sqrt{s} = 5.02$ TeV is compared to predictions based on the canonical statistical hadronisation model (CSM) described in [68], as a function of the multiplicity of particles produced in the collision, expressed in terms of the average pseudorapidity density of charged particles, $\langle dN_{ch}/d\eta \rangle$. The prediction spans a large $\langle dN_{ch}/d\eta \rangle$ interval, reaching the high multiplicity achieved in central heavy-ion collisions at LHC energies. In canonical statistical hadronisation models, hadrons are formed from a source that is assumed to have reached full chemical equilibrium at the chemical freeze-out temperature T_{ch}, and their yields are determined from the partition function for a canonical ensemble. The multiplicity dependence of hadron production is driven by the canonical suppression, namely the exact conservation of baryon number, electric charge, and strangeness over the correlation volume. The model considered here, with a temperature $T_{\mathrm{ch}} = 155$ MeV and a correlation volume that spans three units of rapidity, is able to reproduce the multiplicity dependence of hadron-to-pion ratios of several species over the charged particle multiplicity range covered by the ALICE measurements at the LHC, both qualitatively and quantitatively in most cases (see Fig. 5 of [68]). In addition, to describe the multiplicity dependence of the ϕ/π ratio observed at the LHC, the model, henceforth labelled as $\gamma_S - $CSM, incorporates the incomplete equilibration of strangeness by introducing a strangeness saturation factor $\gamma_S \leq 1$. Notably, in the strangeness nonequilibrium picture a s$\bar{\mathrm{s}}$ pair like the ϕ meson is effectively a double-strange particle ($|S| = 2$), and ALICE ϕ data seem to be best described with $|S| = 1$–2 [69]. The $f_0(980)/\pi^+$ ratio is calculated for two scenarios, first assuming that the total strangeness content of $f_0(980)$ is equal to zero (yellow continuous line) and second, assuming a total strangeness content equal to two (blue dashed line). At high multiplicity, where the strangeness content of the system saturates in presence of a QGP, the calculations for the two scenarios converge and reach the grand canonical limit.

In the first scenario ($|S| = 0$), γ_s-CSM predicts higher values for the $f_0(980)$ to pion yield ratio as compared to the second scenario ($|S| = 2$) in the low $\langle dN_{\mathrm{ch}}/d\eta \rangle$ region. The two predictions match each other for $\langle dN_{\mathrm{ch}}/d\eta \rangle \geq 100$. The measured $2f_0/(\pi^+ + \pi^-)$ ratio in pp collisions at $\sqrt{s} = 5.02$ TeV

differs by 1.9σ from the γ_s-CSM prediction for the $f_0(980)$ with net strangeness equal to zero, and by 4.0σ from the $|S| = 2$ prediction, indicating that the former scenario is favoured over the latter in this implementation of the model.

5   Conclusions

In conclusion, the first measurement of $f_0(980)$ production in inelastic pp collisions at $\sqrt{s} = 5.02$ TeV at the LHC is presented. The measurement is performed in a wide p_T interval from 0 to 16 GeV/c at midrapidity by reconstructing the resonance in the hadronic decay channel $f_0(980) \rightarrow \pi^+\pi^-$. The inclusive $f_0(980)$ production is underestimated by HERWIG 7.2 by a factor of two for $1 < p_T < 4$ GeV/c and by a large factor (up to more than four) in $4 < p_T < 16$ GeV/c. However, this QCD-inspired event generator is able to describe the p_T-dependence of the $2f_0(980)/(\pi^+ +\pi^-)$ and $f_0(980)/\phi$ ratios in a rather broad p_T range, while failing to reproduce the $2f_0(980)/(p+\overline{p})$ ratio over the entire measured p_T range. The production of $f_0(980)$ is also not described by a AMPT+coalescence model prediction in three configurations ($s\overline{s}$ meson, $u\overline{u}s\overline{s}$ tetraquark state, and K^+K^- molecule), which use the phase space information of quarks and kaons from the AMPT model. In order to compare the new measurement of the p_T-integrated $f_0(980)$ to pion ratio with low energy data, the low energy points were updated with the latest branching ratio. The new result presented in this letter suggests a mild increase of the production of $f_0(980)$ relative to pions in inelastic pp collisions from $\sqrt{s} = 27.5$ GeV to $\sqrt{s} = 5.02$ TeV. For the same ratio, HERWIG 7.2 predicts a value that is about 43% lower than the measured one whereas different implementations of the statistical hadronisation model underestimate the data by up to a factor of about two. Notably, the γ_s-CSM prediction for the $f_0(980)$ assuming net strangeness equal to zero is consistent with the data within 1.9σ.

In summary, the description of the inclusive f_0 production in pp collisions provided by the few event generators and theoretical calculations that attempt its modelling is, at present, unsatisfactory. Future developments in this direction may help gaining insight over the nature of this particle, as new data may become available. From the experimental point of view, the results presented in this letter set the necessary baseline for the future measurements of the production and the nuclear modification factor of $f_0(980)$ in p–Pb and Pb–Pb collisions at the LHC, which have been suggested as observables that are sensitive to the elusive nature of this particle.

References

[1] M. Gell-Mann, "A Schematic Model of Baryons and Mesons", *Phys. Lett.* **8** (1964) 214–215.

[2] **Particle Data Group** Collaboration, P. Zyla *et al.*, "Review of Particle Physics", *PTEP* **2020** no. 8, (2020) 083C01.

[3] R. L. Jaffe, "Multi-Quark Hadrons. 1. The Phenomenology of (2 Quark 2 anti-Quark) Mesons", *Phys. Rev. D* **15** (1977) 267.

[4] R. L. Jaffe, "Multi-Quark Hadrons. 2. Methods", *Phys. Rev. D* **15** (1977) 281.

[5] F. E. Close and N. A. Tornqvist, "Scalar mesons above and below 1-GeV", *J. Phys. G* **28** (2002) R249–R267, arXiv:hep-ph/0204205.

[6] C. Amsler and N. A. Tornqvist, "Mesons beyond the naive quark model", *Phys. Rept.* **389** (2004) 61–117.

[7] L. Maiani, F. Piccinini, A. D. Polosa, and V. Riquer, "A New look at scalar mesons", *Phys. Rev. Lett.* **93** (2004) 212002, arXiv:hep-ph/0407017.

[8] E. Klempt and A. Zaitsev, "Glueballs, Hybrids, Multiquarks. Experimental facts versus QCD inspired concepts", *Phys. Rept.* **454** (2007) 1–202, `arXiv:0708.4016 [hep-ph]`.

[9] **Particle Data Group** Collaboration, M. A. Amsler C., Eidelman S. and V. G., "Review of Particle Physics: Spectroscopy of Light Meson Resonances", *PTEP* **2020** no. 8, (2020) 083C01.

[10] C.-H. Chen, "Evidence for two quark content of f(0)(980) in exclusive b —> c decays", *Phys. Rev. D* **67** (2003) 094011, `arXiv:hep-ph/0302059`.

[11] N. N. Achasov, J. V. Bennett, A. V. Kiselev, E. A. Kozyrev, and G. N. Shestakov, "Evidence of the four-quark nature of f_0(980) and f_0(500)", *Phys. Rev. D* **103** no. 1, (2021) 014010, `arXiv:2009.04191 [hep-ph]`.

[12] H. A. Ahmed and C. W. Xiao, "Study the molecular nature of σ, f_0(980), and a_0(980) states", *Phys. Rev. D* **101** no. 9, (2020) 094034, `arXiv:2001.08141 [hep-ph]`.

[13] D. Oliinychenko and C. Shen, "Resonance production in PbPb collisions at 5.02 TeV via hydrodynamics and hadronic afterburner", `arXiv:2105.07539 [hep-ph]`.

[14] N. N. Achasov, "Radiative decays of phi meson about nature of light scalar resonances", *Nucl. Phys. A* **728** (2003) 425–438, `arXiv:hep-ph/0309118`.

[15] M. N. Achasov *et al.*, "The phi –> eta pi0 gamma decay", *Phys. Lett. B* **479** (2000) 53–58, `arXiv:hep-ex/0003031`.

[16] **CMD-2** Collaboration, R. R. Akhmetshin *et al.*, "First observation of the phi –> pi+ pi- gamma decay", *Phys. Lett. B* **462** (1999) 371, `arXiv:hep-ex/9907005`.

[17] **KLOE** Collaboration, A. Aloisio *et al.*, "Study of the decay $\phi \to \eta \pi^0 \gamma$ with the KLOE detector", *Phys. Lett. B* **536** (2002) 209–216, `arXiv:hep-ex/0204012`.

[18] **KLOE** Collaboration, F. Ambrosino *et al.*, "Dalitz plot analysis of $e^+ e^- \to \pi^0 \pi^0 \gamma$ events at $\sqrt{s}$ approximately M(ϕ) with the KLOE detector", *Eur. Phys. J. C* **49** (2007) 473–488, `arXiv:hep-ex/0609009`.

[19] **BESIII** Collaboration, M. Ablikim *et al.*, "Amplitude analysis of the $\pi^0 \pi^0$ system produced in radiative J/ψ decays", *Phys. Rev. D* **92** no. 5, (2015) 052003, `arXiv:1506.00546 [hep-ex]`. [Erratum: Phys.Rev.D 93, 039906 (2016)].

[20] **E791** Collaboration, E. M. Aitala *et al.*, "Study of the D$_s^+ \to \pi^- \pi^+ \pi^+$ decay and measurement of f(0) masses and widths", *Phys. Rev. Lett.* **86** (2001) 765–769, `arXiv:hep-ex/0007027`.

[21] **LHCb** Collaboration, R. Aaij *et al.*, "Measurement of resonant and CP components in $\bar{B}_s^0 \to J/\psi \pi^+ \pi^-$ decays", *Phys. Rev. D* **89** no. 9, (2014) 092006, `arXiv:1402.6248 [hep-ex]`.

[22] **LHCb** Collaboration, R. Aaij *et al.*, "Measurement of the resonant and CP components in $\bar{B}^0 \to J/\psi \pi^+ \pi^-$ decays", *Phys. Rev. D* **90** no. 1, (2014) 012003, `arXiv:1404.5673 [hep-ex]`.

[23] J. T. Daub, C. Hanhart, and B. Kubis, "A model-independent analysis of final-state interactions in $\bar{B}_{d/s}^0 \to J/\psi \pi\pi$", *JHEP* **02** (2016) 009, `arXiv:1508.06841 [hep-ph]`.

[24] G. Janssen, B. C. Pearce, K. Holinde, and J. Speth, "On the structure of the scalar mesons f0 (975) and a0 (980)", *Phys. Rev. D* **52** (1995) 2690–2700, `arXiv:nucl-th/9411021`.

[25] J. D. Weinstein and N. Isgur, "K anti-K Molecules", *Phys. Rev. D* **41** (1990) 2236.

[26] C. W. Xiao, U. G. Meißner, and J. A. Oller, "Investigation of $J/\psi \to \gamma\pi^0\eta(\pi^+\pi^-, \pi^0\pi^0)$ radiative decays including final-state interactions", *Eur. Phys. J. A* **56** no. 1, (2020) 23, arXiv:1907.09072 [hep-ph].

[27] L. Maiani, A. D. Polosa, V. Riquer, and C. A. Salgado, "Counting valence quarks at RHIC and LHC", *Phys. Lett. B* **645** (2007) 138–145, arXiv:hep-ph/0606217.

[28] **ExHIC** Collaboration, S. Cho *et al.*, "Exotic hadrons from heavy ion collisions", *Prog. Part. Nucl. Phys.* **95** (2017) 279–322, arXiv:1702.00486 [nucl-th].

[29] A. Gu, T. Edmonds, J. Zhao, and F. Wang, "Elliptical flow coalescence to identify the $f_0(980)$ content", *Phys. Rev. C* **101** no. 2, (2020) 024908, arXiv:1902.07152 [nucl-ex].

[30] **HotQCD** Collaboration, A. Bazavov *et al.*, "Chiral crossover in QCD at zero and non-zero chemical potentials", *Phys. Lett. B* **795** (2019) 15–21, arXiv:1812.08235 [hep-lat].

[31] **ALICE** Collaboration, K. Aamodt *et al.*, "Two-pion Bose-Einstein correlations in central Pb-Pb collisions at $\sqrt{s_{NN}}$ = 2.76 TeV", *Phys. Lett. B* **696** (2011) 328–337, arXiv:1012.4035 [nucl-ex].

[32] **ALICE** Collaboration, S. Acharya *et al.*, "Production of the $\rho(770)^0$ meson in pp and Pb-Pb collisions at $\sqrt{s_{NN}}$ = 2.76 TeV", *Phys. Rev. C* **99** no. 6, (2019) 064901, arXiv:1805.04365 [nucl-ex].

[33] **ALICE** Collaboration, S. Acharya *et al.*, "Evidence of rescattering effect in Pb–Pb collisions at the LHC through production of K$^*(892)^0$ and $\phi(1020)$ mesons", *Phys. Lett. B* **802** (2020) 135225, arXiv:1910.14419 [nucl-ex].

[34] **ALICE** Collaboration, S. Acharya *et al.*, "Suppression of $\Lambda(1520)$ resonance production in central Pb-Pb collisions at $\sqrt{s_{NN}}$ = 2.76 TeV", *Phys. Rev. C* **99** (2019) 024905, arXiv:1805.04361 [nucl-ex].

[35] R. J. Fries, B. Muller, C. Nonaka, and S. A. Bass, "Hadronization in heavy ion collisions: Recombination and fragmentation of partons", *Phys. Rev. Lett.* **90** (2003) 202303, arXiv:nucl-th/0301087.

[36] V. Minissale, F. Scardina, and V. Greco, "Hadrons from coalescence plus fragmentation in AA collisions at energies available at the BNL Relativistic Heavy Ion Collider to the CERN Large Hadron Collider", *Phys. Rev. C* **92** no. 5, (2015) 054904, arXiv:1502.06213 [nucl-th].

[37] S. Plumari, V. Minissale, S. K. Das, G. Coci, and V. Greco, "Charmed Hadrons from Coalescence plus Fragmentation in relativistic nucleus-nucleus collisions at RHIC and LHC", *Eur. Phys. J. C* **78** no. 4, (2018) 348, arXiv:1712.00730 [hep-ph].

[38] **ALICE** Collaboration, B. B. Abelev *et al.*, "Performance of the ALICE Experiment at the CERN LHC", *Int. J. Mod. Phys. A* **29** (2014) 1430044, arXiv:1402.4476 [nucl-ex].

[39] **ALICE** Collaboration, K. Aamodt *et al.*, "The ALICE experiment at the CERN LHC", *JINST* **3** (2008) S08002.

[40] **ALICE** Collaboration, E. Abbas *et al.*, "Performance of the ALICE VZERO system", *JINST* **8** (2013) P10016, arXiv:1306.3130 [nucl-ex].

[41] **STAR** Collaboration, C. Adler *et al.*, "Coherent ρ^0 production in ultraperipheral heavy ion collisions", *Phys. Rev. Lett.* **89** (2002) 272302, arXiv:nucl-ex/0206004.

[42] **ALICE** Collaboration, J. Adam *et al.*, "Coherent ρ^0 photoproduction in ultra-peripheral Pb-Pb collisions at $\sqrt{s_{\mathrm{NN}}} = 2.76$ TeV", *JHEP* **09** (2015) 095, arXiv:1503.09177 [nucl-ex].

[43] S. Stone and L. Zhang, "Use of $B \to J/\psi f_0$ decays to discern the $q\bar{q}$ or tetraquark nature of scalar mesons", *Phys. Rev. Lett.* **111** no. 6, (2013) 062001.

[44] **ALICE** Collaboration, "ALICE luminosity determination for pp collisions at $\sqrt{s} = 5$ TeV", *ALICE-PUBLIC-2016-005* (2016) .

[45] C. Loizides, J. Kamin, and D. d'Enterria, "Improved Monte Carlo Glauber predictions at present and future nuclear colliders", *Phys. Rev.* **C97** no. 5, (2018) 054910, arXiv:1710.07098 [nucl-ex]. [Erratum: Phys. Rev.C99,no.1,019901(2019)].

[46] P. Skands, S. Carrazza, and J. Rojo, "Tuning PYTHIA 8.1: the Monash 2013 Tune", *Eur. Phys. J. C* **74** no. 8, (2014) 3024, arXiv:1404.5630 [hep-ph].

[47] R. Brun, F. Bruyant, F. Carminati, S. Giani, M. Maire, A. McPherson, G. Patrick, and L. Urban, "GEANT Detector Description and Simulation Tool", *CERN-W-5013* (10, 1994) .

[48] **ALICE** Collaboration, S. Acharya *et al.*, "Transverse momentum spectra and nuclear modification factors of charged particles in pp, p-Pb and Pb-Pb collisions at the LHC", *JHEP* **11** (2018) 013, arXiv:1802.09145 [nucl-ex].

[49] **ALICE** Collaboration, J. Adam *et al.*, "Measurement of pion, kaon and proton production in proton–proton collisions at $\sqrt{s} = 7$ TeV", *Eur. Phys. J. C* **75** no. 5, (2015) 226, arXiv:1504.00024 [nucl-ex].

[50] J. Bellm *et al.*, "Herwig 7.0/Herwig++ 3.0 release note", *Eur. Phys. J. C* **76** no. 4, (2016) 196, arXiv:1512.01178 [hep-ph].

[51] M. Bahr *et al.*, "Herwig++ Physics and Manual", *Eur. Phys. J. C* **58** (2008) 639–707, arXiv:0803.0883 [hep-ph].

[52] Z.-W. Lin, C. M. Ko, B.-A. Li, B. Zhang, and S. Pal, "A Multi-phase transport model for relativistic heavy ion collisions", *Phys. Rev. C* **72** (2005) 064901, arXiv:nucl-th/0411110.

[53] B.-A. Li and C. M. Ko, "Formation of superdense hadronic matter in high-energy heavy ion collisions", *Phys. Rev. C* **52** (1995) 2037–2063, arXiv:nucl-th/9505016.

[54] B. Li, A. T. Sustich, B. Zhang, and C. M. Ko, "Studies of superdense hadronic matter in a relativistic transport model", *Int. J. Mod. Phys. E* **10** (2001) 267–352.

[55] X.-N. Wang and M. Gyulassy, "HIJING: A Monte Carlo model for multiple jet production in p p, p A and A A collisions", *Phys. Rev. D* **44** (1991) 3501–3516.

[56] B. Zhang, "ZPC 1.0.1: A Parton cascade for ultrarelativistic heavy ion collisions", *Comput. Phys. Commun.* **109** (1998) 193–206, arXiv:nucl-th/9709009.

[57] B. Andersson, G. Gustafson, and B. Soderberg, "A General Model for Jet Fragmentation", *Z. Phys. C* **20** (1983) 317.

[58] B. Andersson, G. Gustafson, G. Ingelman, and T. Sjöstrand, "Parton Fragmentation and String Dynamics", *Phys. Rept.* **97** (1983) 31–145.

[59] T. Sjöstrand, "High-energy physics event generation with PYTHIA 5.7 and JETSET 7.4", *Comput. Phys. Commun.* **82** (1994) 74–90.

[60] Z.-w. Lin and C. M. Ko, "Partonic effects on the elliptic flow at RHIC", *Phys. Rev. C* **65** (2002) 034904, `arXiv:nucl-th/0108039`.

[61] **ALICE** Collaboration, S. Acharya *et al.*, "Production of charged pions, kaons, and (anti-)protons in Pb–Pb and inelastic pp collisions at $\sqrt{s_{\mathrm{NN}}}$ = 5.02 TeV", *Phys. Rev. C* **101** no. 4, (2020) 044907, `arXiv:1910.07678 [nucl-ex]`.

[62] W. Hofmann, "Particle Composition in Hadronic Jets in e^+e^- Annihilation", *Ann. Rev. Nucl. Part. Sci.* **38** (1988) 279–322.

[63] P. V. Chliapnikov, "Hyperfine Splitting in Light-Flavour Hadron Production at LEP", *Phys. Lett. B* **462** (1999) 341–353.

[64] M. Aguilar-Benitez *et al.*, "Inclusive particle production in 400-GeV/c pp interactions", *Z. Phys. C* **50** (1991) 405–426.

[65] F. Becattini, P. Castorina, J. Manninen, and H. Satz, "The Thermal Production of Strange and Non-Strange Hadrons in e^+e^- Collisions", *Eur. Phys. J. C* **56** (2008) 493–510, `arXiv:0805.0964 [hep-ph]`.

[66] F. Becattini and U. W. Heinz, "Thermal hadron production in p p and p anti-p collisions", *Z. Phys. C* **76** (1997) 269–286, `arXiv:hep-ph/9702274`. [Erratum: Z.Phys.C 76, 578 (1997)].

[67] A. Andronic, P. Braun-Munzinger, K. Redlich, and J. Stachel, "Decoding the phase structure of QCD via particle production at high energy", *Nature* **561** no. 7723, (2018) 321–330, `arXiv:1710.09425 [nucl-th]`.

[68] V. Vovchenko, B. Dönigus, and H. Stoecker, "Canonical statistical model analysis of p-p , p -Pb, and Pb-Pb collisions at energies available at the CERN Large Hadron Collider", *Phys. Rev. C* **100** no. 5, (2019) 054906, `arXiv:1906.03145 [hep-ph]`.

[69] **ALICE** Collaboration, B. B. Abelev *et al.*, "K*(892)^0 and ϕ(1020) production in Pb-Pb collisions at $\sqrt{s_{\mathrm{NN}}}$ = 2.76 TeV", *Phys. Rev. C* **91** (2015) 024609, `arXiv:1404.0495 [nucl-ex]`.